THERMODYNAMICALLY BASED MOISTURE PREDICTION USING ROE'S SCHEME

M. J. Kermani[1], **A. G. Gerber**[2], **J. M. Stockie**[3]
University of New Brunswick
Fredericton, New Brunswick, Canada, E3B 5A3
M.Kermani@unb.ca

Abstract

Isentropic expansion of subsonic-supersonic moist steam flow in 1D converging–diverging nozzles is studied numerically. The equilibrium thermodynamic model has been used to predict moisture generation. To discretize the convective terms, Roe's density-based scheme has been used. For dry regions, the pressure (p), temperature (T), and velocity (u) are extrapolated to cell faces by the MUSCL approach using a third-order upwind-biased scheme, while in wet regions T, u and the quality (χ) are used for extrapolation purposes. Pressure in moist regions is, therefore, equated to saturation pressure at the local temperature. The Roe-averaged value at the cell faces is obtained based on mixture (liquid + vapor) properties at the sides of the cell faces. The van Albada flux limiter is used to prevent spurious numerical oscillations.

Keywords: Steam Flow – Equilibrium Thermodynamics – Moisture Prediction – CFD

Introduction

Correct prediction of moisture levels in multi-phase wet flow applications is a vital issue. Condensing flow occurs in a wide range of industrial applications, from low speed flows such as fuel cells, to high speed cases such air/steam mixtures in air breathing engines, and steam flow through the components of steam power plant turbines.

The development of non-equilibrium multiphase flow models begins with the knowledge of the equilibrium state. For example in non-equilibrium condensation predictions in transonic flow devices such steam turbines, the equilibrium state is required for the estimation of the homogeneous nucleation parameters, [1, 2, 3]. Results pertaining to moisture generated homogeneously or heterogeneously under non-equilibrium flow conditions can be validated in the limit against equilibrium moisture predictions. Moisture predictions using an equilibrium model combined with the high-order Roe scheme are presented in this paper. This work sets the stage for subsequent implementation of multiphase condensation models where non-equilibrium nucleation models are considered.

Governing Equations

The governing equations of fluid motion for quasi one-dimensional, unsteady, compressible flow in full conservative form with no body force can be written as (see Ref. [4]):

$$\frac{\partial}{\partial t}(SQ) + \frac{\partial F}{\partial x} - H_s = 0, \tag{1}$$

[1]Postdoctoral Fellow, Departments of Mechanical Engineering and Mathematics and Statistics
[2]Associate Professor, Department of Mechanical Engineering
[3]Assistant Professor, Department of Mathematics and Statistics

where x and t are the space and time coordinates, S is the cross sectional area of the duct, Q, F, and H_s respectively represent, the conservative vector, the flux vector and the source term, given by:

$$Q = \begin{bmatrix} \rho \\ \rho u \\ \rho e_t \end{bmatrix}, \qquad F = S \begin{bmatrix} \rho u \\ \rho u^2 + p \\ \rho u H \end{bmatrix}, \qquad H_s = \frac{dS}{dx} \begin{bmatrix} 0 \\ p \\ 0 \end{bmatrix}.$$

Here, ρ is the mixture density (vapor + liquid), u the velocity, e_t the total mixture energy, p the pressure, and H the total mixture enthalpy. For the present study of low pressure steam flow at below one atmosphere, the ideal gas equation of state

$$p = \rho_g RT \tag{2}$$

is of sufficient accuracy, in which ρ_g is the gas density and R is the gas constant (= 461.3990 J/kg.K for vapor). In dry regions ρ_g is the same as mixture density, while in wet regions $\rho_g = \rho\chi$, where χ is the quality of the mixture (i.e., the mass fraction of the vapor to that of the mixture). It is noted in the present study the volume of the liquid is assumed to be much smaller than that of the vapor, and hence is ignored. In the present computation h_{fg} (enthalpy of evaporation) is obtained as follows:

$$h_{fg} = e_{fg} + RT \tag{3}$$

where e_{fg} is the change in internal energy from the saturated liquid state to that of the saturated vapor. A second order polynomial can accurately represent the relationship between e_{fg} and T, and the coefficients are provided in Appendix A. The internal energy of the vapor, e_g, is determined assuming a constant value for the specific heat at constant volume, i.e.

$$e_g = C_v T, \tag{4}$$

where $C_v = R/(\gamma - 1)$, with $\gamma = 1.32$ for vapor. Equation 4 provides the saturated vapor internal energy with $e_g = C_v T_{sat}$, where can be used to obtain the saturated liquid internal energy e_f

$$e_f = e_g(T_{sat}) - e_{fg}. \tag{5}$$

In the present study, entropy is used only for post-processing purposes, and its calculation is addressed in Appendix A.

Time Discretization

For the time discretization, an explicit, two-step scheme belonging to the Lax-Wendroff family of predictor-corrector methods has been used to step the solution from time level n to $n + 1$ (see for example [5]). The predictor step determines the flow conditions at an intermediate step (time level $n + 1/2$):

$$\frac{1}{\Delta t/2}\left[(SQ)^{n+1/2} - (SQ)^n\right] + \frac{1}{\Delta x}\left[F_E^n - F_W^n\right] - H_s^n = 0, \tag{6}$$

where F_E^n and F_W^n are the numerical fluxes evaluated at the East (E) and West (W) faces of the control volume, the evaluation of which are addressed in the next section.

The predictor step is followed by the corrector step, which is a central differencing in time around $n + 1/2$ implemented as follows:

$$\frac{1}{\Delta t}\left[(SQ)^{n+1} - (SQ)^n\right] + \frac{1}{\Delta x}\left[F_E^{n+1/2} - F_W^{n+1/2}\right] - H_s^{n+1/2} = 0. \tag{7}$$

Space Discretization

The spatial discretization for the numerical scheme is determined by the formulae used to compute the numerical fluxes on cell faces. In the present computation, a third order upwind-biased algorithm with the MUSCL extrapolation strategy [6] is applied to obtain Left (L) and Right (R) values for the flow conditions at cell faces. In this approach, the nodal values are assumed to be known and extrapolation provides values on both sides of each cell

face. In the present study, the L and R values are used to obtain the so-called Roe's averaged conditions at the cell faces (see [7]).

Various parameters are used in the literature for extrapolation purposes (see for example [8]), including conservative vectors (Q), primitive variables (p, ρ, T, u, etc.) or flux vectors (F), and we use primitive variables in the present study.

For the dry region, cell face values for the primitive variables p, T, and u can uniquely determine the state point. However, for the computation of wet cell faces, pressure and temperature are not independent parameters, and the quality, (χ), is extrapolated to the cell face instead of pressure. Therefore, local pressure is equated to the saturation pressure at the local temperature.

The third order extrapolation scheme used in the present computation is:

$$\begin{aligned} q_E^L &= q_j + \frac{1}{4}[(1-\kappa)\Delta_W q + (1+\kappa)\Delta_E q], \\ q_E^R &= q_{j+1} - \frac{1}{4}[(1-\kappa)\Delta_{EE} q + (1+\kappa)\Delta_E q], \end{aligned} \tag{8}$$

where q represents one of p, u, T if the flow is dry at the cell faces; otherwise q represents T, u, or χ. In these formulae, $\kappa = 1/3$ corresponding to the third order upwind biased scheme, $\Delta_W q = q_j - q_{j-1}$, $\Delta_E q = q_{j+1} - q_j$, and $\Delta_{EE} q = q_{j+2} - q_{j+1}$.

Roe's Averaging for Wet Flow Computation

The numerical flux for Roe's scheme is calculated at the so-called Roe's averaged value obtained from the L and R states on both sides of a cell face. For dry flow conditions, this has been well explained in several texts (see for example [5] or [9]). For wet flow conditions, it should be noted that gas properties are taken to be those of the mixture; for example, density and total enthalpy at the Roe's averaged condition are obtained for the East face of a control volume by:

$$\hat{\rho}_{_E} = \sqrt{\rho_{_E}^{L}\ \rho_{_E}^{R}} \tag{9}$$

$$\hat{H}_{_E} = \frac{\sqrt{\rho_{_E}^{L}} H_{_E}^{^L} + \sqrt{\rho_{_E}^{R}} H_{_E}^{^R}}{\sqrt{\rho_{_E}^{L}} + \sqrt{\rho_{_E}^{R}}} \tag{10}$$

where all the properties in wet regions correspond to the mixture values. For example,

$$\rho_E^L = (\rho_g)_E^L \ /\ (\chi)_E^L \tag{11}$$

where $\rho_g = p_{sat}/(RT)$ for wet flow, and

$$H_E^L = \underbrace{(h_f)_E^L \ +\ (\chi)_E^L\ (h_{fg})_E^L}_{\text{mixture enthalpy}} \ +\ \frac{1}{2}\left[(u)_E^L\right]^2. \tag{12}$$

Flux Limiter

Spurious numerical oscillations are unavoidable in these high resolution computations, but can be prevented using the van Albada flux limiter [10]. This limiter has been reported and implemented in various forms in the literature (see [8] and [11]). The following form of van Albada's limiter has been used in the present work (and in previously reported results [12]), and has been shown to prevent spurious numerical oscillations and give better convergence [13, 14]:

$$\begin{aligned} q_E^L &= q_j + \frac{\phi_j}{4}[(1-\kappa)\Delta_W q + (1+\kappa)\Delta_E q], \\ q_E^R &= q_{j+1} - \frac{\phi_{j+1}}{4}[(1-\kappa)\Delta_{EE} q + (1+\kappa)\Delta_E q]. \end{aligned} \tag{13}$$

The limiter function, ϕ, is a function of forward- and backward-differences defined by:

$$\phi_j \equiv \frac{2(\Delta_W q)(\Delta_E q) + \epsilon}{(\Delta_W q)^2 + (\Delta_E q)^2 + \epsilon}, \tag{14}$$

and ϵ is a small parameter that prevents indeterminacy in regions of zero gradients, i.e. where $(\Delta_W q) = (\Delta_E q) = 0$.

Entropy Correction

Roe's scheme incorrectly captures expansion shocks in the regions where eigenvalues of the Jacobian matrix of flux vector vanish. These regions are sonic regions or stagnation points. To avoid expansion shocks from appearing in these regions, several entropy correction formulae were reported in the literature, with one of the most popular being that of Harten and Hyman (see Ref. [15]). A modified version of this formula which totally eliminates expansion shocks from sonic expansion regions without affecting the rest of the domain (see Ref. [16]) has been used:

$$\begin{cases} \hat{\lambda}_{new} \leftarrow (\hat{\lambda}^2 + \epsilon^2) \,/\, 2\,\epsilon, & \text{if } |\lambda| < \epsilon, \\ |\lambda| < \epsilon & \\ \epsilon = 4.0\ \max\left[0, \left(\hat{\lambda} - \lambda^L\right), \left(\lambda^R - \hat{\lambda}\right)\right], & \text{otherwise}, \end{cases} \tag{15}$$

where $\hat{\lambda}$ is the eigenvalue of the Jacobian flux matrix determined at Roe's averaged condition, and λ^L and λ^R are the eigenvalues determined at L or R flow conditions respectively.

Speed of Sound

An accurate estimate of the speed of sound is essential for time-varying upwind algorithms such as the one we employ here. This is because the wave speeds (or the eigenvalues of the Jacobian matrix of the flux vector), $\lambda_{1,2,3}$ = u, $u + c$, and $u - c$, determine the directions along which information propagates within the $x - t$ plane. For dry, single-phase flow, the speed of sound is a well-established thermodynamic property given by:

$$a^2 = \left(\frac{\partial p}{\partial \rho}\right)_s, \tag{16}$$

where s is the mixture entropy (see Appendix A). Unfortunately, the speed of sound is not so easily determined in wet flows, and in general it cannot be treated as a thermodynamic property (see Ref. [17]). However, for steam flow obeying a thermodynamic equilibrium model, speed of sound can be approximated as a thermodynamic property obtained from Eqn. 16. Obtaining the speed of sound from Eqn. 16 is a cumbersome task, and therefore using it as part of an iterative algorithm is not efficient.

Alternatively, Guha (1995) has proposed the following algebraic equation to conveniently obtain the speed of sound for wet steam flows in equilibrium thermodynamic models (see [17]):

$$a^2 = \frac{\chi\gamma RT}{\gamma\left[1 - RT/h_{fg}(2 - CT/h_{fg})\right]}, \tag{17}$$

where $C = C_p + (1 - \chi)\, C_l \,/\chi$. The quantities C_p and C_l are the specific heat values at saturation vapor and liquid, respectively. It is noted that Eqn. 17 is used only for wet steam flows under equilibrium conditions.

Another approach to calculating the speed of sound is using the so-called frozen value, which is determined based on the gas side values only. In other words, the presence of moisture is ignored when the speed of sound is calculated, so that the wet and dry phases are treated as two independent phases. This approach leads to:

$$a^2 = \gamma RT. \tag{18}$$

Figure 1 contains a plot of the speed of sound obtained along an isobar process sweeping from the dry state to the wet state. As shown in this figure, the frozen value of the speed of sound matches very well with that obtained

by Eqn. 16 in the dry region; furthermore, the formulation provided by Guha (Eqn. 17), completely overlaps to that of Eqn. 16 in wet region. There is no single formulation capturing the speed of sound in both dry and wet regions, and the formula of Eqn. 16 is not a computationally efficient choice. However, the speed of sound can only affect the solution in the transient region, and the steady-state solution is not sensitive to the choice of a. The sensitivity of the steady-state solution to the frozen speed of sound $\pm$ 20 % has been tested in the present study, and no changes have been observed in the steady state results. Consequently, for the present computation containing both dry and wet regions with our interest being only on the steady-state solution, the frozen value of speed of sound (i.e. Eqn. 18) has been used.

Moisture Evaluation

As the solution marches in time, the conservative vector Q is obtained at each time level. Q provides values for mixture density and total internal energy. Knowing the value of velocity at the same time level, a static value of the internal energy can be obtained. The thermodynamic state point can then be fixed based on current values of mixture density and internal energy. The moisture content (if present) for this equilibrium state can then be determined.

Boundary Conditions

The inflow is subsonic and assumed to be dry, for which the stagnation pressure and temperature are specified. At the exit plane for which supersonic conditions prevail, all flow properties are extrapolated from the interior domain.

Numerical Validation; Comparison vs. Experimental Values

To validate the results of the present computation, two nozzle geometries are chosen, labeled as nozzles (A) and (D) in Fig. 1-(Right). The computed pressure distributions along the nozzle axis are compared with those from experiments of Ref. [18] using nozzles (A) and (D). Nozzle (A) has the highest expansion rate of these series of nozzles (i.e. the largest exit to throat area ratio) and nozzle (D) has the lowest expansion rate. The flow conditions are: $P_{0_{in}}$=25 kPa taken constant for all the nozzles geometries, $T_{0_{in\,A}}$=354.6 K, and $T_{0_{in\,D}}$=361.8 K. The outflow conditions for all cases are supersonic.

Figure 2-(Left) and (Right) compare the computed pressure distributions along the nozzle with the experimental values obtained for nozzles (A) and (D). As shown in these figures the agreement between the computation and experiment are quite good, with differences between them owing to different choked mass flows through the nozzles which we explain as follows. Rapid expansion through the nozzles forces the flow to experience non-equilibrium conditions in real (experimental) case. Therefore condensation in the experiment does not begin until a significant amount of supercooling is achieved. This delays the moisture generation in the experiment, and it can be shown that flow is still dry in the nozzle throat if non-equilibrium model is used (see [19]). In our computations, assuming moisture formation under equilibrium conditions, the flow is moist at the nozzle throat (see Fig. 3-(Left)) which causes the choked mass flow rate to differ slightly from the experiments.

The slight rise in the pressure (see experimental data in Fig. 2-(Left) is attributed to a condensation shock. A complete study of non-equilibrium steam flow through these nozzles and capturing the condensation shock was performed earlier and reported in Ref. [19].

Results

Stagnant flow introduced at an imaginary reservoir upstream of the inflow plane is accelerated to the inlet boundary. This flow is continuously accelerated along the nozzle and crosses the saturation line, say at point S (see Fig. 3). A uniform profile for each of the mixture mass ($\dot{m}$), mixture total enthalpy (h_t) and mixture entropy (s_m) has been obtained along the nozzle at the converged state, (see Fig. 4 for h_t and s_m profile). The mixture mass flow profile along the nozzle is also perfectly uniform (not shown here) with a value of

$$|\dot{m}_{out} - \dot{m}_{in}|/\dot{m}_{in} < 0.0008. \tag{19}$$

According to the equilibrium model, moisture is generated as soon as the saturation line is crossed. Unlike the dry flow case where the inflow boundary condition determines mass flow through a given nozzle, in the wet flow computation the amount of moisture at the throat is also important and reduces the choked mass flow. Using the present equilibrium model, the mass flow rate in nozzle (A) with p_{0in} =25 kPa and T_{0in} = 354.6 K is computed as 1.2627 kg/s. However, the choked mass flow rate under dry conditions is given by

$$(\dot{m}_{max})_{dry} = \frac{p_0 A^*}{\sqrt{(RT_0)}} \sqrt{\gamma \left(\frac{2}{\gamma+1}\right)^{\frac{\gamma+1}{\gamma-1}}}, \tag{20}$$

yielding a value of 1.3069 kg/s which is an overestimate of $\approx 3.5\%$.

As noted earlier, Fig. 4-(Left) and (Right) depict the enthalpy and entropy profiles along the nozzle (A) axis at the converged state. Point S in these figures corresponds to the saturated vapor state. As shown in Fig. 4-(Left) total enthalpy (denoted by h_t) is uniform along the nozzle axis, showing that the energy equation is well satisfied. Also shown in this figure is the mixture enthalpy, h_m, which decreases as the flow accelerates along the nozzle with increasing kinetic energy. Mixture entropy is also uniform, as shown in Fig. 4-(Right), representing an isentropic process through the nozzle.

Figure 5 shows the Mach number profile along the nozzle axis obtained based on the frozen value of the speed of sound. The Mach number at the nozzle throat is not unity because flow is wet at the throat and therefore the speed of sound differs from its frozen value (see Fig. 1). It should be noted that the Mach number (pictured in Fig. 5) is a post-processing parameter having no effect on the actual computation.

Conclusion

A method for the computation of moisture content in subsonic-supersonic steam flow has been described based on an equilibrium thermodynamic model, implemented using Roe's scheme. Primitive variables p, T and u are extrapolated to the cell faces in dry regions, while in wet regions T, u and χ are used. Pressure in moist regions is, therefore, equated to saturation pressure at the local temperature. Roe's averaged values are obtained based on mixture properties at the cell faces.

The method is not limited to a single-component approach, and can be extended to condensing multi-species flows such as air/steam mixtures. The results compare well versus experimental results on non-equilibrium condensation where the effect of throat moisture levels on choked mass flow is considered. The choked mass flow through a nozzle, unlike the dry flow case, cannot be determined directly based only on inflow stagnation conditions, nozzle geometry and fluid properties (Eqn. 20). In addition, the moisture content at the throat also affects the mass flow rate through the duct relative to a non-equilibrium prediction when moisture formation is delayed until a location beyond the throat.

Appendix A

Saturation Pressure. The saturation pressure for steam is determined by a fifth order polynomial least square curve fit to the steam data taken from [20], given by:

$$p_{sat} = A_5(T-t_0)^5 + A_4(T-t_0)^4 + A_3(T-t_0)^3 + A_2(T-t_0)^2 + A_1(T-t_0) + A_0, \tag{21}$$

where p and T are in terms of Pa and K, $t_0 = 273.15$, accurately predicting saturation pressure in the range of $T = [293, 423]$ K. The coefficients are

$$\begin{aligned} A_5 &= +1.777491E-6 \\ A_4 &= +5.81810511E-4 \\ A_3 &= -8.508110796E-3 \\ A_2 &= +3.282638938134E+0 \\ A_1 &= +1.313809434459E+0 \\ A_0 &= +9.63591656226039E+2 \end{aligned} \tag{22}$$

Internal Energy. Internal energy is obtained by a parabolic curve fit to the steam data taken from [20], as

$$e_{fg} = E_2(T - t_0)^2 + E_1(T - t_0) + E_0, \tag{23}$$

where e_{fg} and T are in terms of J/kg and K, and

$$\begin{aligned} E_2 &= -0.00000196412464E + 6 \\ E_1 &= -0.00266166511681E + 6 \\ E_0 &= +2.37267810643234E + 6 \end{aligned} \tag{24}$$

Therefore, $h_{fg} = e_{fg} + RT$, where R=461.3990 $J/kg.K$ for vapor.

Entropy. The entropy of the mixture is determined from $s = s_f + \chi s_{fg}$, where $s_{fg} = h_{fg}/T$ and s_g is obtained from $s_g = C_p \ln T - R \ln p$, and $s_f = s_g - s_{fg}$.

Acknowledgment

Financial support for this research were provided by Natural Sciences and Engineering Research Council of Canada (NSERC) and the MITACS Network of Centers of Excellence.

References

[1] Gerber, A.G. "Two-Phase Eulerian/Lagrangian Model for Nucleating Steam Flow", Journal of Fluids Engineering, vol. 124, June 2002.

[2] White, A. J., and Young, J. B., "Time-Marching Method for the Prediction of Two-Dimensional, Unsteady Flows of Condensing Steam", Journal of Propulsion and Power, Vol. 9, No. 4, pp. 579-587, July-Aug. 1993.

[3] Bakhtar, F., Mahpeykar, M.R., Abbas, K.K., "An Investigation of Nucleating Flows of Steam in a Cascade of Turbine Blading - Theoretical Treatment", ASME J. Fluids Eng., vol. 117, pp.138-144, 1995^b.

[4] Hoffmann, K. A. and Chiang, S. T., "Computational Fluid Dynamics for Engineers", Vol. II, A Publication of Engineering Education Systems, Wichita, Kansas, USA, 1993.

[5] Tannehill, J. C., Anderson, D. A., Pletcher, R. H., Computational Fluid Mechanics and Heat Transfer, Second Edition, 1997.

[6] van Leer, B., "Towards the Ultimate Conservation Difference Scheme, V, A Second Order Sequel to Godunov's Method", J. Comput. Phys., Vol. 32, pp. 110-136, 1979.

[7] Roe, P. L., "Approximate Riemann Solvers, Parameter Vectors and Difference Schemes" J. Comput. Phys., Vol. 43, pp 357-372, 1981.

[8] Thomas, J. L., and Walters, R. W. "Upwind Relaxation Algorithms for Navier-Stokes Equations", AIAA J., Vol. 25, pp 527-537, 1987.

[9] Hirsch, C., "Numerical Computation of Internal and External Flows", Wiley, Vol 2, 1990.

[10] van Albada, G. D., van Leer, B., and Roberts, W. W., "A Comparative Study of Computational Methods in Cosmic Gas Dynamics", Astron. Astrophys., Vol. 108, pp 76-84, 1982.

[11] Amaladas, J. R., "Implicit, multigrid and Local-Preconditioning Procedures for Euler and Navier-Stokes Computations with Upwind Schemes", Department of Aerospace Engineering, Indian Institute of Technology, Bangalore, India, June 1995.

[12] Kermani, M. J., ”Development and Assessment of Upwind Schemes with Application to Inviscid and Viscous Flows on Structured Meshes”, Ph.D. thesis, Department of Mechanical & Aerospace Engineering, Carleton University, Canada, 2001.

[13] Amaladas, J. R., private communication, Indian Institute of Technology, Bangalore, India, March 2000.

[14] Thomas, J. L., private communication, NASA Langley, March 2000.

[15] Harten, A., Hyman, J. M., ”Self-Adjusting Grid Methods for One-Dimensional Hyperbolic Conservation Laws”, Journal of Comput. Physics, Vol. 50, pp 235-269, 1983.

[16] Kermani, M. J. and Plett, E. G. ”Modified Entropy Correction Formula for the Roe Scheme”, AIAA 2001-0083.

[17] Guha, A., ”Two-Phase Flows with Phase Transition”, von Karman Institute Lecture Series 1995-06, May 29–June 1, 1995.

[18] Moore, M.J., Walters, P.T., Crane, R.I., and Davidson, B.J., ”Predicting the Fog Drop Size in Wet Steam Turbines”, Inst. of Mechanical Engineers (UK), Wet Steam 4 Conf., University of Warwick, paper C37/73, 1973.

[19] Kermani, M. J., and Gerber, A. G., ”Thermodynamic and Aerodynamic Loss Evaluation of Supersonic Nucleating Steam Flow with Shocks”, ASME Paper # FEDSM2002-31087, ASME Fluids Engineering Division, Montreal, Canada, July 14-18, 2002.

[20] Moran, M. J., and Shapiro, H. N., ”Fundamentals of Engineering Thermodynamics”, 4^{th} Edition, John Wiley & Sons, 1998.

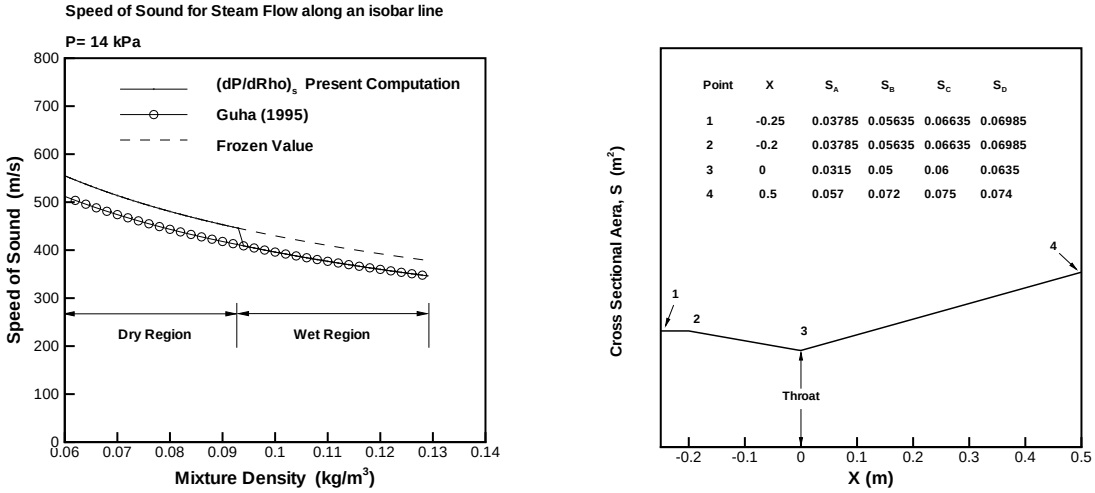

Figure 1: (Left)- A typical profile of speed of sound along an isobar line, determined in three different ways and (Right)- geometry of nozzles used in the present computations.

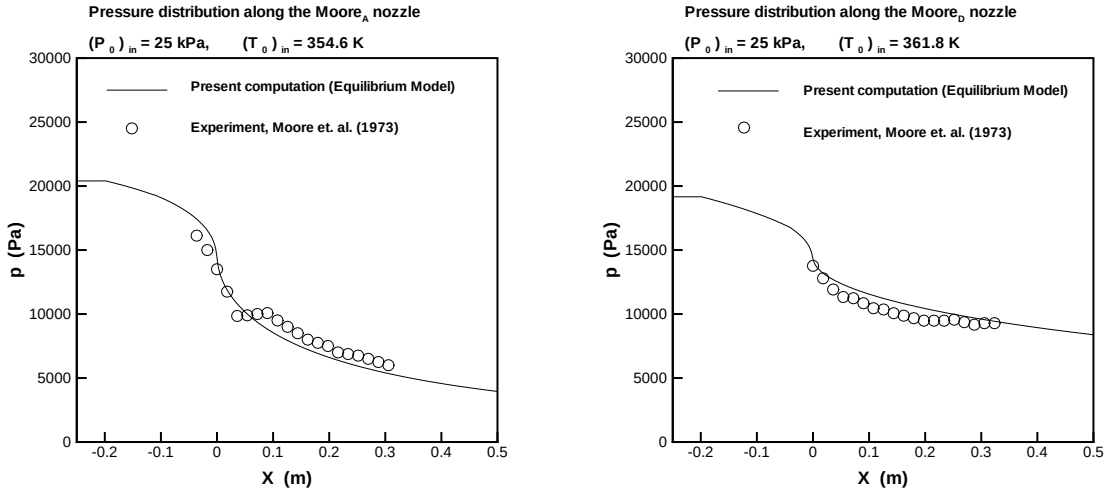

Figure 2: Comparison of pressure distribution along the nozzle centerline (Left)- nozzle Moore$_A$ and (Right)- nozzle Moore$_D$.

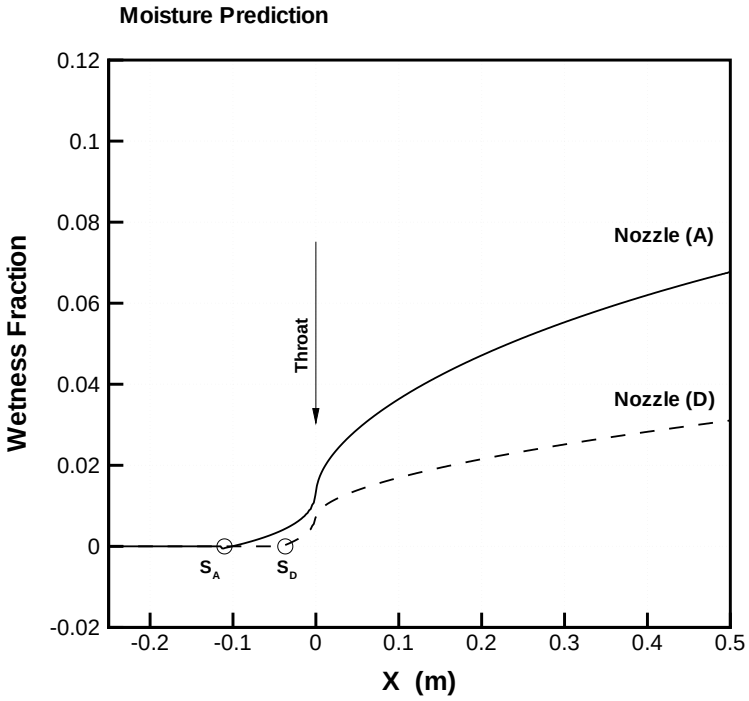

Figure 3: Moisture prediction along the nozzles axes; S_A and S_D correspond to the saturation vapor (moisture onset) point. Flow is wet at the nozzle throat (x=0) according to the equilibrium model.

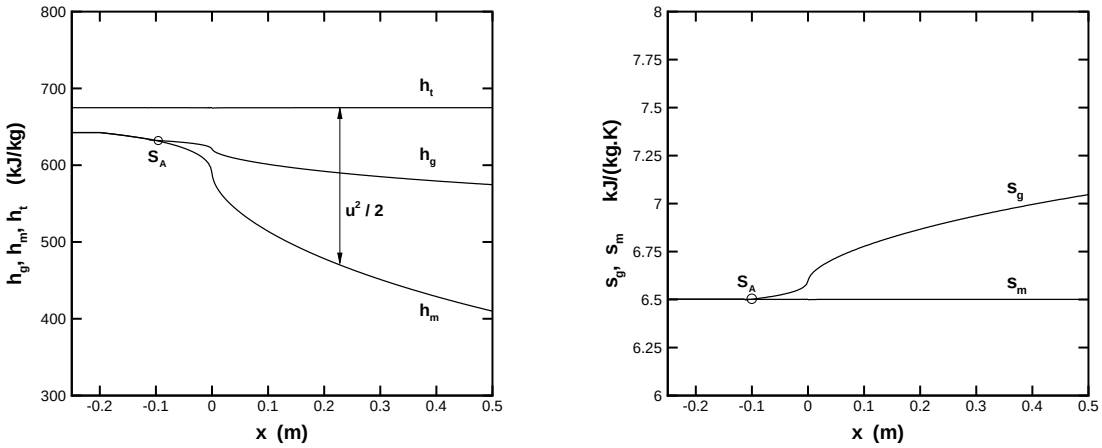

Figure 4: (Left)- Profile of mixture, total and gas side enthalpy at the converged state, and (Right)- Profile of mixture and gas side entropy at the converged state. Point S corresponds to a saturated vapor state.

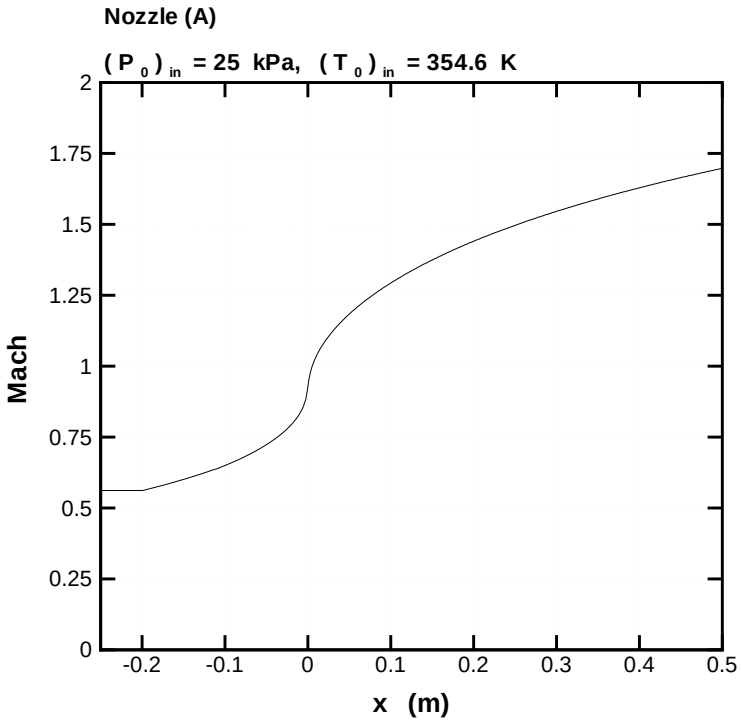

Figure 5: The Mach number profile along the nozzle axis based on a frozen speed of sound. The value of the Mach number at the throat is not unity, because the speed of sound differs from its frozen value.